NANO MICRO small

# Supporting Information

for *Small,* DOI: 10.1002/smll.202203045

## Ionic Conductive and Highly-Stable Interface for Alkali Metal Anodes

*Enzhong Jin, Karnpiwat Tantratian, Changtai Zhao, Anastasia Codirenzi, Lyudmila V. Goncharova, Changhong Wang, Feipeng Yang, Yijia Wang, Parham Pirayesh, Jinghua Guo, Lei Chen,* Xueliang Sun,* and Yang Zhao**

# Supporting Information

## Ionic Conductive and Highly-Stable Interface for Alkali Metal Anode

*Enzhong Jin[1+], Karnpiwat Tantratian[2+], Changtai Zhao[1], Anastasia Codirenzi[4], Lyudmila V. Goncharova[4], Changhong Wang[1], Feipeng Yang[3], Yijia Wang[1], Parham Pirayesh[1], Jinghua Guo[3], Lei Chen[2, 5*], Xueliang Sun[1*], Yang Zhao[1*]*

[1]Department of Mechanical and Materials Engineering
University of Western Ontario, London, Ontario, N6A 5B9, Canada
Email: X. Sun: xsun9@uwo.ca; Y. Zhao: yzhao628@uwo.ca

[2]Department of Mechanical Engineering
University of Michigan−Dearborn, Dearborn, Michigan 48128, United States
Email: L. Chen: leichn@umich.edu

[3]Advanced Light Source
Lawrence Berkeley National Laboratory, Berkeley, CA, 94720, United States

[4]Department of Physics and Astronomy
University of Western Ontario, London, Ontario, N6A 3K7, Canada

[5]Michigan Institute for Data Science
University of Michigan, Ann Arbor, Michigan 48109, United States

+ These authors contribute equally to this work

## Materials and Methods

**LiAlOx coating fabrication:** Two types of Li foils with different thicknesses (350 μm and 40 μm) were used, which were stored in the argon-filed glove box. ALD $Al_2O_3$ coatings were conducted in a Gemstar-8 ALD system (Arradiance, USA) directly connected with the argon-filed glove box. For the ALD $Al_2O_3$ process, trimethylaluminium (TMA) and water ($H_2O$) were used as precursors. The ALD process used as 0.1 s/30 s/0.1 s/50 s TMA pulse/purge/ $H_2O$ pulse/purge sequence. To study the ALD deposition temperature effects, the deposition temperatures of ALD $Al_2O_3$ were controlled at 120 $^oC$ (below the melting point) and 180 $^oC$ (close to the melting point), in which the samples are named as Li@n$Al_2O_3$ and Li@nLiAlOx-in (n=ALD cycles), respectively. To achieve the high quality $LiAlO_x$ coating, the two-step approach was further developed. In this two-step approach, the ALD $Al_2O_3$ was first deposited on Li metal at the regular temperature of 120 $^oC$. Then, the ALD chamber was heated up to 180 $^oC$ for the post-treatment and kept for half an hour. The samples obtained by this ex-situ process are named as Li@nLiAlOx-ex (n=ALD cycles).

**NaAlOx coating fabrication:** A fresh Na foil with the diameter of 3/8 inch was prepared with the aid of a homemade press machine by pressing a piece of sodium metal stick (from Aldrich) as a starting sodium metal. The ALD $Al_2O_3$ coating for Na metal was deposited using the similar recipe above at the deposition temperature of 65 $^oC$. The as-deposited sample is named as Na@n$Al_2O_3$ (n=ALD cycles). Then, the ALD chamber was heated up to the melting point of Na metal of 98 $^oC$ and kept for half an hour to obtain the $NaAlO_x$ coating. The sample is named as Na@n$NaAlO_x$ (n=ALD cycles).

**Electrochemical measurements:** The electrochemical performance was analyzed in CR2032 coin-type cells. The coin cells were assembled in an ultra-pure argon-filled glove box by symmetrical Li/electrolyte-separator/Li system using polypropylene separator (Celgard 2400). The electrolyte used for symmetrical cell is carbonate-based electrolyte (1 M $LiPF_6$ in EC: DEC: DMC with 10 % FEC). The electrolyte amount used for all the samples were ~ 30 uL. The stripping/plating studies were carried out on a Land 2001A Battery Test System and Neware Battery Test System at room temperature. A constant current was applied to the electrodes during repeated stripping/plating while the potential was recorded over time in the symmetric cell testing. The thickness of Li for optimizing the coating thickness is 350 μm. Li-$LiFePO_4$(LFP) batteries were tested via CR2032 cells using bare Li foil and protected Li (Li@200LiAlOx-ex) with carbonate-based electrolyte (1M $LiPF_6$ in EC:DEC:DMC with 10 % FEC). The Li foil used for

full cells testing was the thick Li foil with the thickness of 350 μm. C/LFP was used as the cathode material. The LFP electrodes were prepared by casting a N, N-Dimethylformamide (NMP) slurry containing C/LFP, Super P and poly(vinylidene difluoride) (PVDF) in a weight ratio of 8:1:1 onto carbon-coated Al foil. The cathodes were cut into discs with a diameter of 10 mm and dried at 80 $^{o}$C prior to use. The areal loading of LFP is about 8-10 mg $cm^{-2}$. The electrolyte amount used for Li-LFP batteries were ~ 30 uL.

Li-$O_2$ batteries were tested via CR2016 cells using pristine Li and protected Li (Li@200LiAlOx-ex) and carbon-based cathode with ether-based electrolyte (1 M $LiCl_4$ in tetraethylene glycol dimethyl ether (TEGDME)). The cathode electrodes of N-doped carbon nanotube (NCNTs) grown on carbon paper (CP) were synthesized via ALD and chemical vapor deposition (CVD) process based on our previous work [1]. The Li foil used for Li-$O_2$ cell was the thick Li foil with the thickness of 350 μm. The electrochemical performance was measured in 1 atm $O_2$ at room temperature.

The symmetrical cell were assembled by symmetrical Na/electrolyte-separator/Na configuration using polypropylene separators (Celgard 3501). The electrolyte used in this study is 1 m sodium triflate ($NaSO_3CF_3$ 98%, Sigma-Aldrich) dissolved in diethylene glycol dimethyl ether (reagent grade ≈98%, Sigma-Aldrich, predried before usage). The Na stripping/plating studies were carried out in an Arbin BT-2000 Battery Test System at room temperature. Constant current densities were applied to the electrodes during repeated stripping/plating while the potential was recorded over time.

**Characterization**: The X-ray diffraction (XRD) patterns of the samples were recorded at 2θ ranging from 10° to 90° on a Bruker AXS D8 Advance with Cu Kα radiation (λ = 1.54178 Å). The batteries were first disassembled in the glovebox and then gently rinsed with dimethyl carbonate to remove residual Li salts and electrolyte. The electrodes were sealed with the Ar-filled tubes before characterization. SEM images were taken using a Hitachi 3400N Environmental SEM at an acceleration voltage of 5 kV.

Rutherford Backscattering Spectroscopy (RBS) spectra were obtained using 2.5 MeV $He^{++}$ ions at the Tandetron accelerator facility at Western University with a Si detector positioned at 170$^{o}$ in Cornell geometry. Due to the sensitive nature of these samples, Li and Na samples were handled in Ar-filled dry bag, before they were introduced to RBS vacuum chamber. Sb-implanted amorphous Si sample with a known Sb content of 4.82 ×$10^{15}$ atoms /$cm^2$ was used for calibration.

The RBS results were then fitted using the MEIS software to determine the elemental depth profile, and diffusion effects of annealing.

ToF-SIMS measurements were conducted using an ION-TOF (GmbH, Germany) ToF-SIMS IV with a bismuth liquid metal ion source in the Surface Science Western. The base pressure of the analysis chamber was ~$10^{-8}$ mbar. The action of the primary ion beam bombardment on the sample surface induces the emission of negative secondary ions. The analysis area was 400 × 400 μm$^2$ (or 500 × 500 μm$^2$). Sputtering with a $Cs^+$ ion beam (3 keV) was used for depth profiling analysis with the sputtering areas of 200 × 200 μm$^2$.

Synchrotron Al K-edge X-ray absorption spectroscopy (XAS) measurements were conducted on Beamline 7.3.1 of the Advanced Light Source at Lawrence Berkeley National Laboratory.

**Phase-field simulation**

**Governing equations:** A non-linear electrochemical phase-field model is utilized to simulate Li dendrite growth behavior in this work [2]. The order parameter ($\xi$) is introduced to describe the phase evolution of Li metal due to the electrodeposition process ($Li^+ + e \rightarrow Li$): $\xi = 1$ refers to the Li metal, $\xi = 0$ refers to the electrolyte phase, while the number in between 0 and 1 implies the interfacial region. The phase evolution, thermodynamically driven by the activation overpoential ($\eta_a$) and Li-ion concentration ($c_+$), is mathematically expressed as

$$\frac{\partial \xi}{\partial t} = -L_\sigma(g'(\xi) - \kappa\nabla^2\xi) - L_\eta h'(\xi)\left\{\exp\left[\frac{(1-\alpha)nF\eta_a}{RT}\right] - c_+\exp\left[\frac{-\alpha nF\eta_a}{RT}\right]\right\}, \quad (1)$$

where $L_\sigma$ and $L_\eta$ are the interface mobility and the reaction-related constant, respectively, $\eta_a = \Delta\phi - E^\Theta$ represents the activation overpotential, where $E^\Theta$ is the standard half-cell potential. The movement of Li-ion concentration ($c_+$) is governed by Nernst-Plank Equation, which essentially describes the movement of Li-ions under diffusion and electrostatic driving forces:

$$\frac{\partial c_+}{\partial t} = \nabla\cdot\left[D^{eff}\nabla c_+ + \frac{D^{eff}c_+}{RT}nF\nabla\phi\right] - \frac{c_s}{c_0}\frac{\partial \xi}{\partial t}, \quad (2)$$

where $D^{eff} = D^e h(\xi) + D^s(1-h(\xi))$ is the effective diffusion coefficient, where $D^e$ and $D^s$ are the Li-ion diffusion coefficients in the electrode and in the electrolyte, respectively. The last term

on the right-hand side of Equation 2 represents the sink of Li-ions due to electrochemical reactions. Lastly, the electric potential ($\phi$) is governed by charge conservation equation, that is

$$\nabla \cdot [\sigma^{eff} \nabla \phi] = I_R, \tag{3}$$

where $\sigma^{eff} = \sigma^e h(\xi) + \sigma^s (1 - h(\xi))$ is the effective conductivity, $\sigma^e$ and $\sigma^s$ are the conductivities of electrode and the electrolyte solutions, respectively. The source term $I_R$ depicts charges entering/leaving due to electrodeposition, having a form of $I_R = nFc_s \partial\xi/\partial t$, where $c_s$ is site density of Li atom.

**Initial/boundary conditions and model implementation: Fig. S26** shows the geometry and initial roughness of Li surface in the simulation. The domain size is 400 x 200 nm, with thickness of a coating layer of 50 nm. The initial thickness of Li metal layer is 5 nm, with two purtubations (representing initial surface roughness). For initial conditions, Li-ion concentration in both electrolyte and coating layer domain is 1 mol/m$^3$. The electric potential in the electrolyte and coating layer is 0.5 V, while in the Li metal domain is 0 V, corresponding to the potential difference across the electrode/electrolyte interface of -0.5 V. The Dirichlet boundary conditions are applied on the top boundary with Li-ion concentration of 1 mol/m$^3$ and the electric potential of 0.5 V, representing the bulk electrolytes. The Li-ion diffusion coefficient of each coating layer is the only parameter that varies. The parameters used in the simulation are listed in **Table S1**. The simulations of Li deposition behavior are carried out on COMSOL Multiphysics 5.5, the finite element software. The adaptive mesh with appropriate grid spacing is chosen to effectively capture the moving interface.

**Table S1**. Simulation parameters

| Parameters | Value | Normalized value |
|---|---|---|
| Reaction constant, $L_\eta$ | $60/s$ | 4000 |
| Interfacial mobility, $L_\sigma$ | 0.33 x 10$^{-6}$ $m^3/Js$ | 2000 |
| Gradient energy coefficient, κ | 1.5 x 10$^{-3}$ $J/m$ | 0.01 |
| Li-ion diffusion (Bare Li), $D^s_{Li+}$ | 4.6 x 10$^{-13}$ $m^2/s$ | 3 |
| Li-ion diffusion ($LiAlO_x$), $D^s_{Li+}$ | 1.4 x 10$^{-11}$ $m^2/s$ | 90 |
| Li-ion diffusion ($Al_2O_3$), $D^s_{Li+}$ | 1.0 x 10$^{-13}$ $m^2/s$ | 0.65 |

| | | |
|---|---|---|
| Li-ion diffusion (Li metal electrode), $D^{e}_{Li+}$ | 1.0 x $10^{-16}$ $m^2/s$ | 0.0006 |
| Electrolyte (and coating) conductivity, $\sigma^{s}$ | 1 $S/m$ | 10 |
| Electrode conductivity, $\sigma^{e}$ | 1 x $10^{7}$ $S/m$ | $10^{9}$ |
| Interfacial energy, $\gamma_N$ | 0.9 $J/m$ | 0.01 |
| Site density of Li metal, $c_s$ | 7.64 x $10^{4}$ $mol/m^3$ | - |

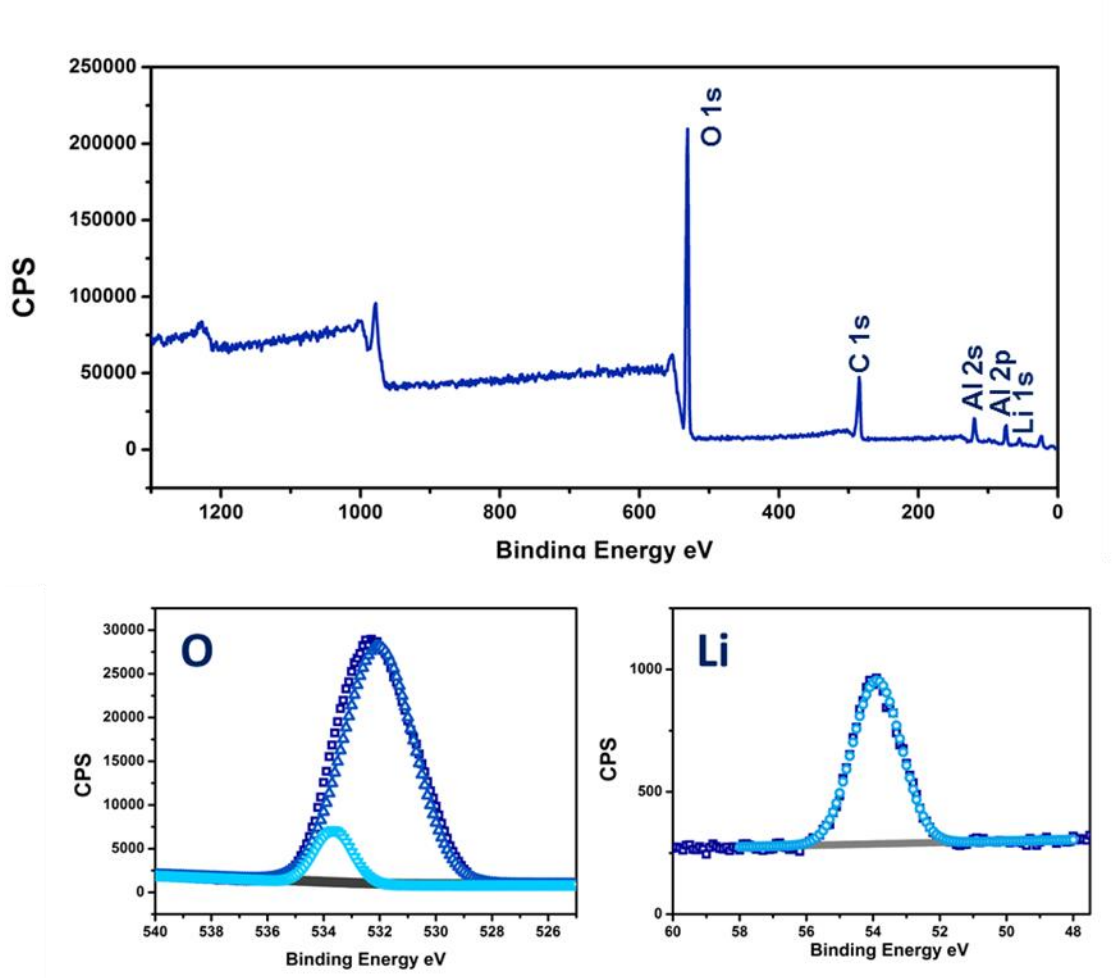


**Fig. S1** The XPS Spectrum of Li@200$Al_2O_3$; high resolution XPS spectra of O 1s and Li 1s of Li@200$Al_2O_3$.

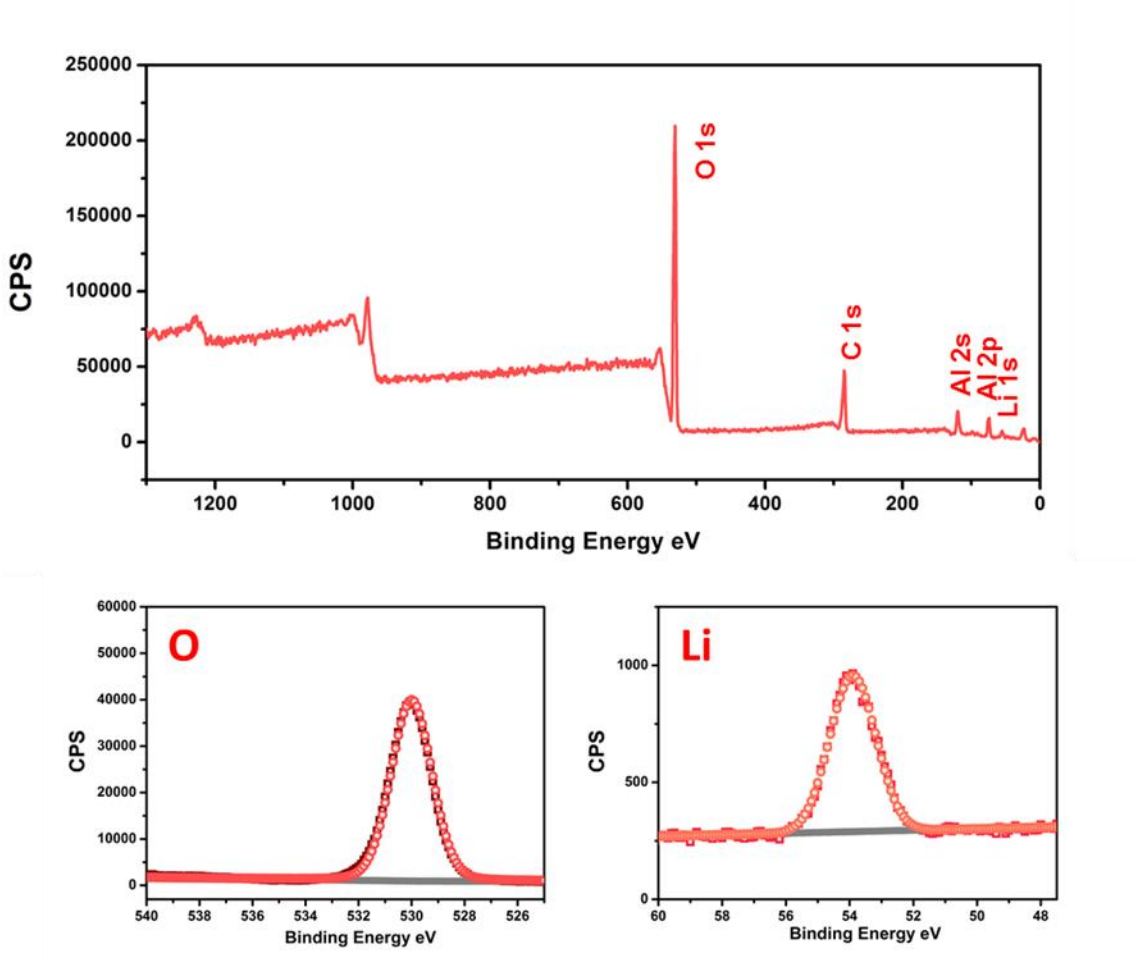


**Fig. S2** The XPS Spectrum of Li@200LiAlO$_x$-ex; high resolution XPS spectra of O 1s and Li 1s of Li@200LiAlO$_x$-ex.

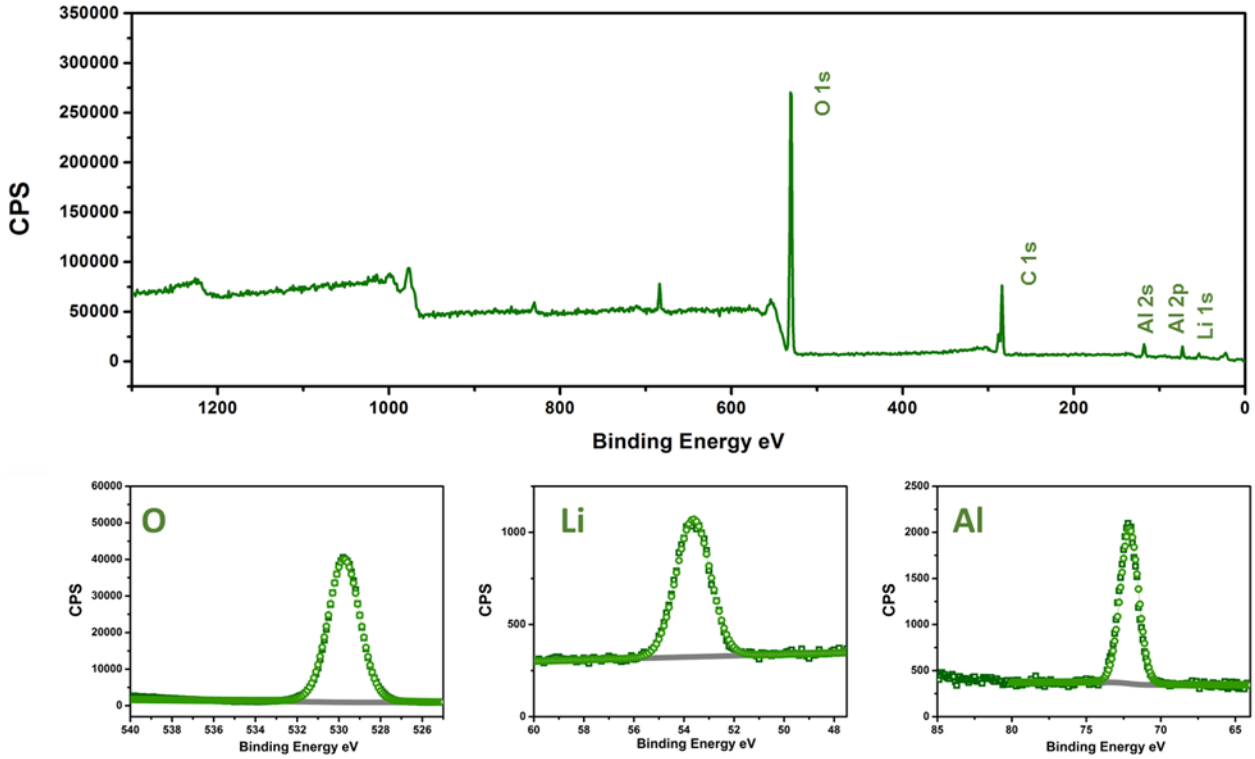


**Fig. S3** The XPS Spectrum of Li@200LiAlO$_x$-in; high resolution XPS spectra of O 1s, Li 1s and Al 2p of Li@200LiAlO$_x$-in.

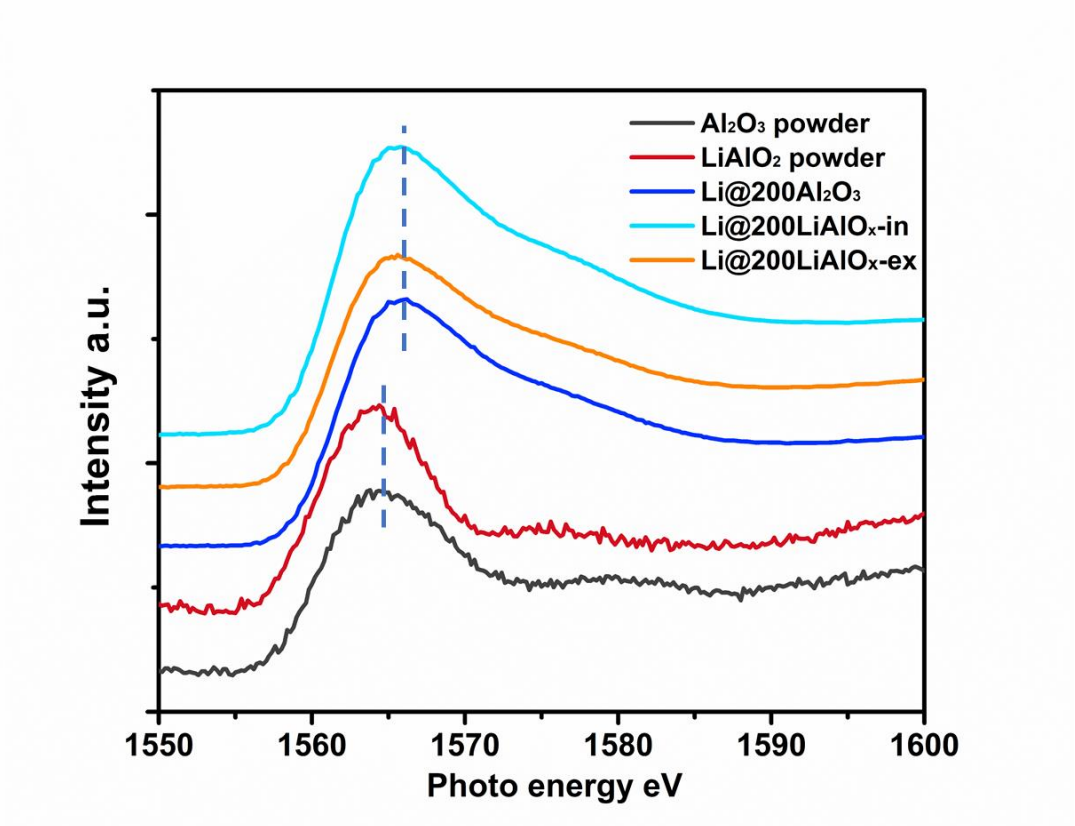


**Fig. S4** The XASENS Al K edge of $Al_2O_3$ powder, $LiAlO_2$ powder, Li@200$Al_2O_3$, Li@200$LiAlO_x$-ex, and Li@200$LiAlO_x$-in.

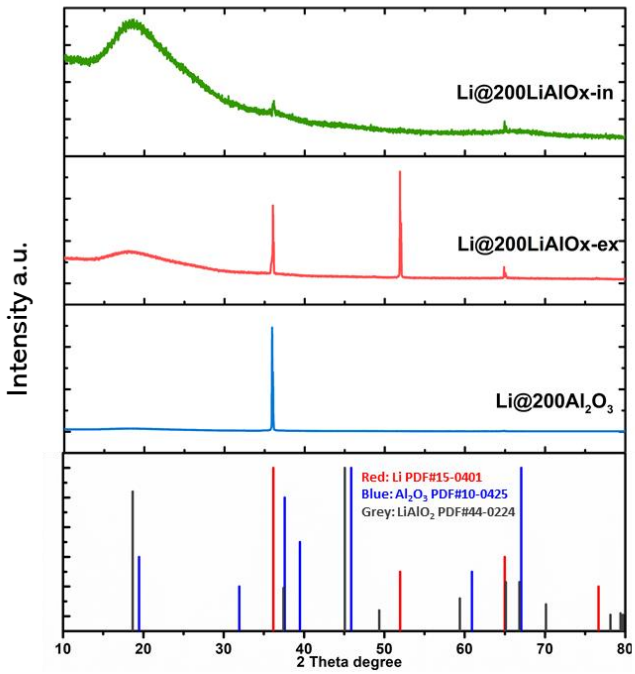


**Fig. S5** The XRD patterns of Li@200$Al_2O_3$, Li@200$LiAlO_x$-ex, and Li@200$LiAlO_x$-in and PDF of Li (PDF#15-0401, Red), $Al_2O_3$ (PDF#10-0425, Blue), $LiAlO_2$ (PDF#44-0224, Grey).

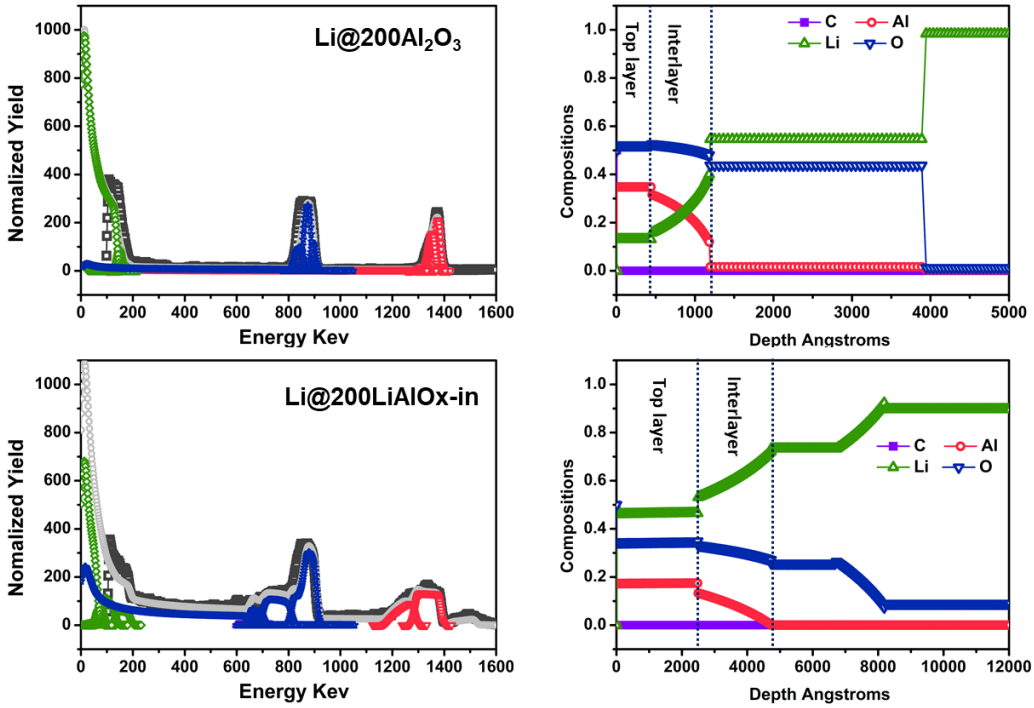


**Fig. S6** The RBS spectra and calculated depth profiles of Li@200$Al_2O_3$ and Li@200$LiAlO_x$-in.

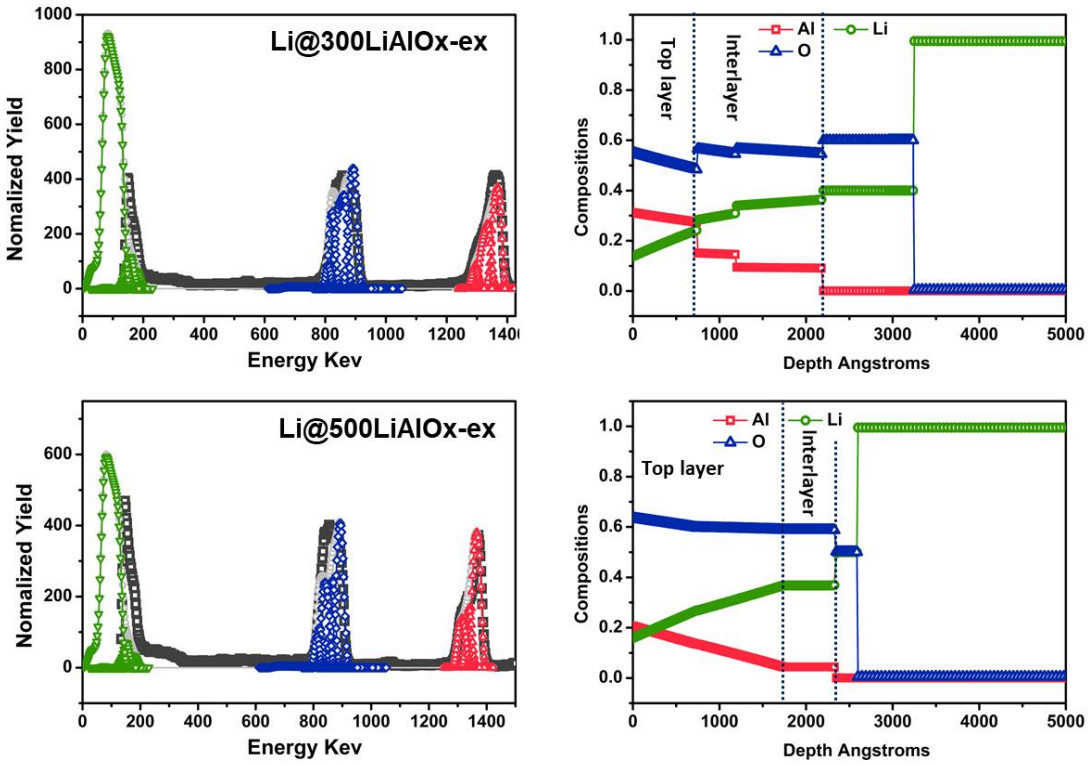


**Fig. S7** The RBS spectra and calculated depth profiles of Li@300LiAlO$_x$-ex and Li@500LiAlO$_x$-ex.

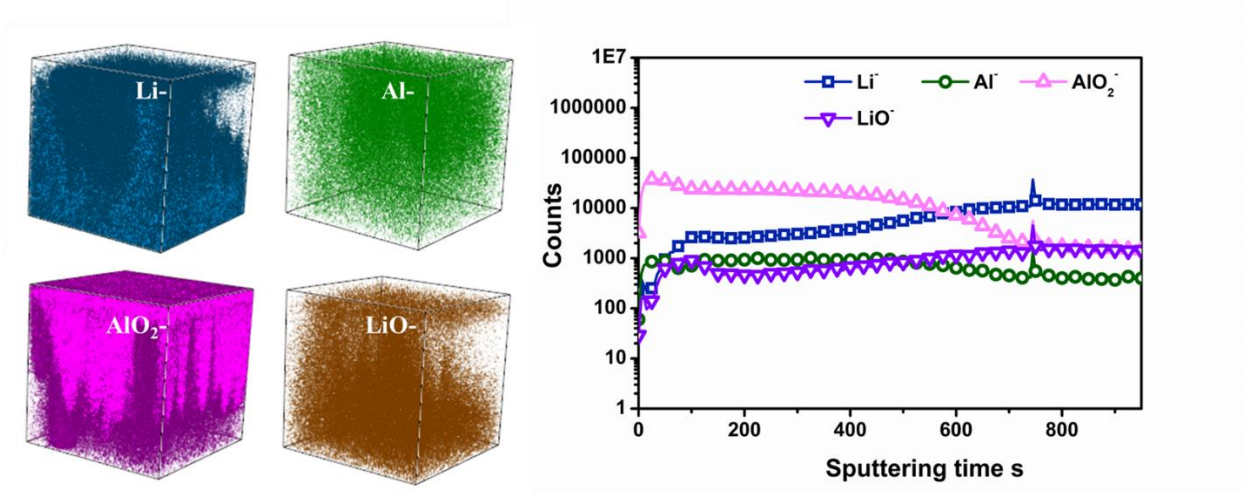


**Fig. S8** The TOF-SIMS secondary ion images, depth profile of various secondary ion species and corresponding 3D images of Li@200LiAlO$_x$-in.

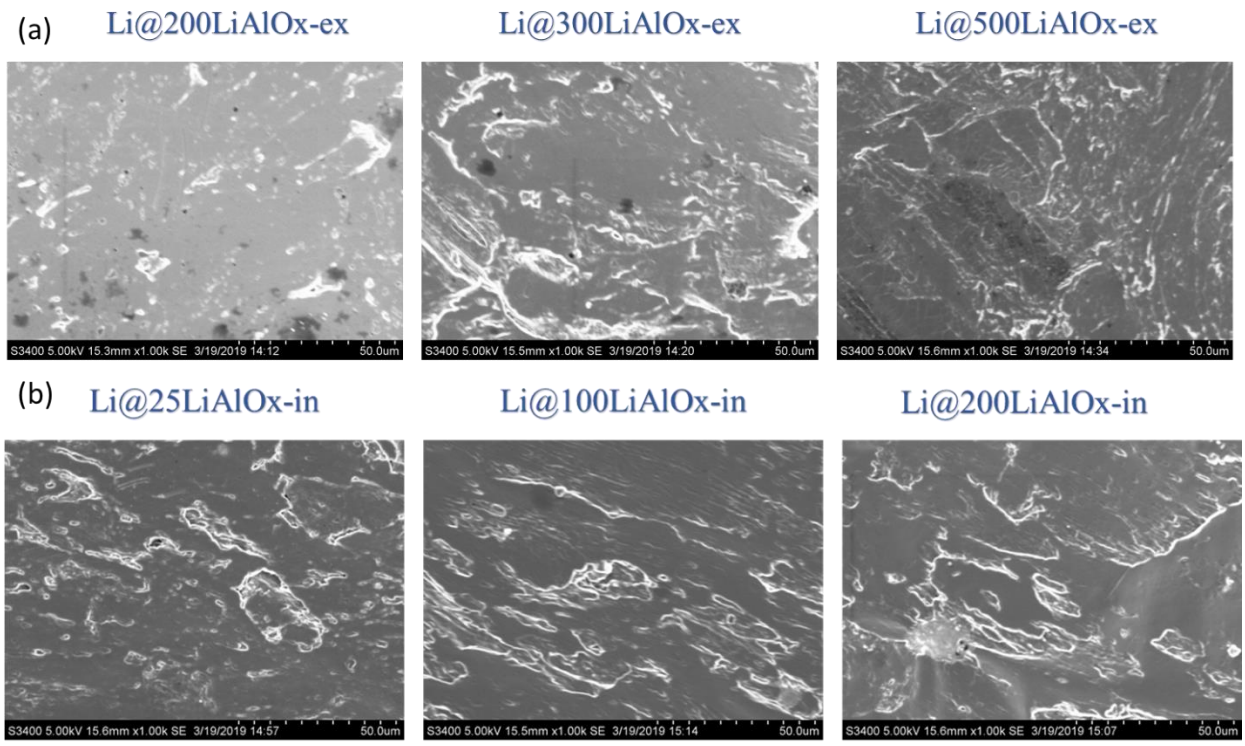


**Fig. S9** Top-view SEM images of (a) 200LiAlO$_x$-ex, Li@300LiAlO$_x$-ex and Li@500LiAlO$_x$-ex; and (b) Li@25LiAlO$_x$-in, Li@100LiAlO$_x$-in and Li@200LiAlO$_x$-in.

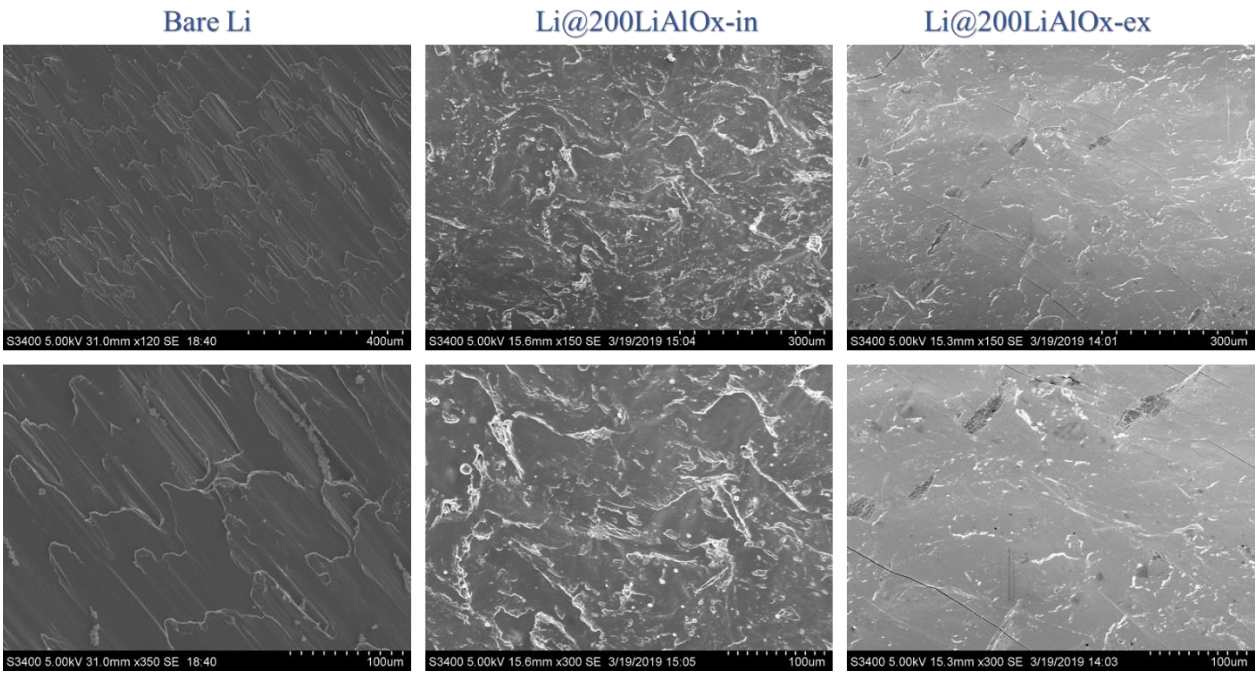


**Fig. S10** Top-view SEM images of bare Li, Li@200LiAl$O_x$-in and Li@200LiAl$O_x$-ex.

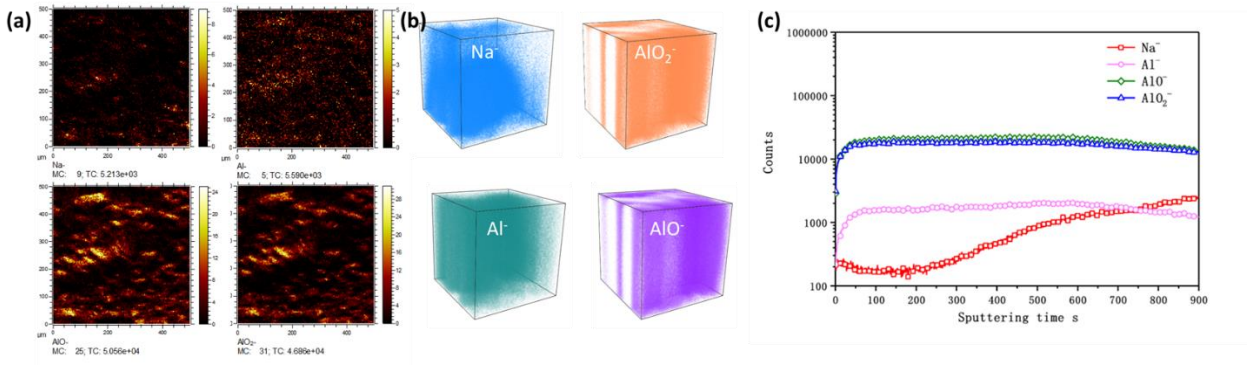


**Fig. S11** The TOF-SIMS surface secondary ion images (a) , depth profile (c) of various secondary ion species and corresponding 3D images (b) of Na@200$Al_2O_3$.

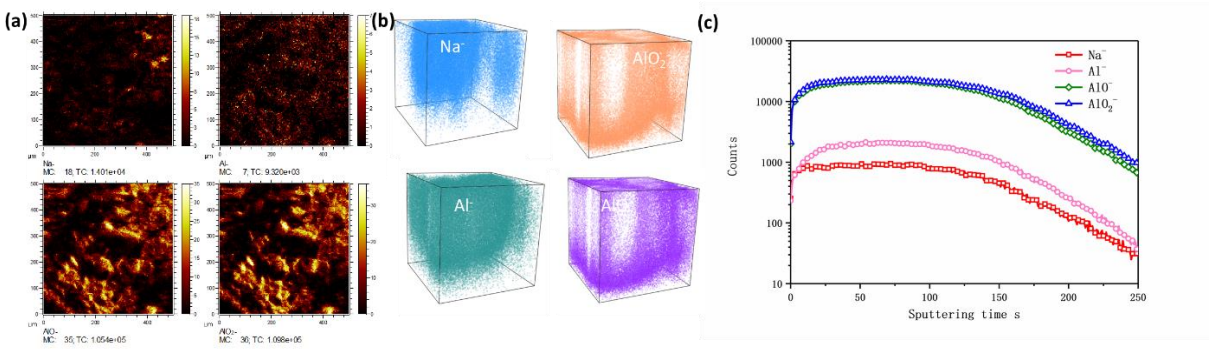


**Fig. S12** The TOF-SIMS surface secondary ion images (a) , depth profile (c) of various secondary ion species and corresponding 3D images (b) of Na@200NaAlO$_x$.

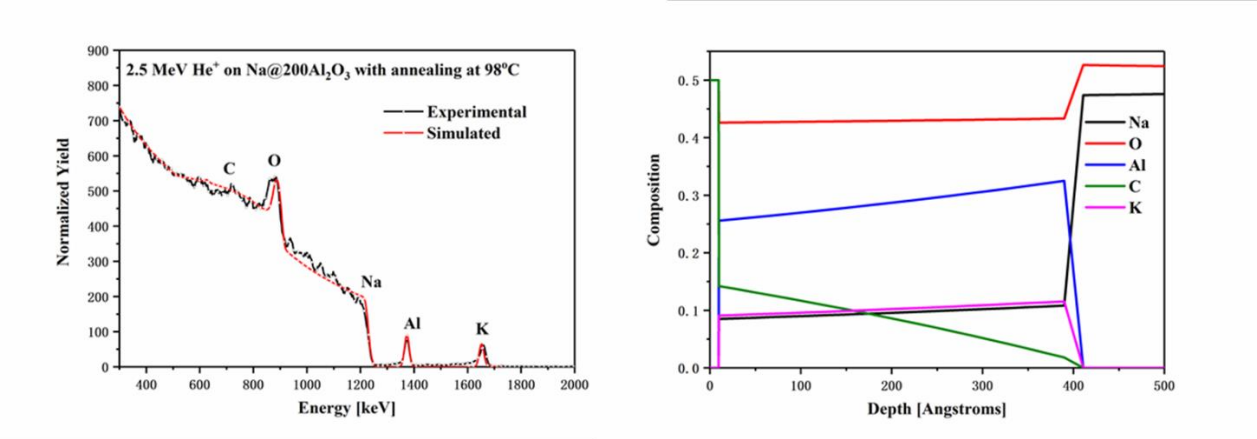


**Fig. S13** The RBS spectra and calculated depth profiles of Na@200NaAl$O_x$

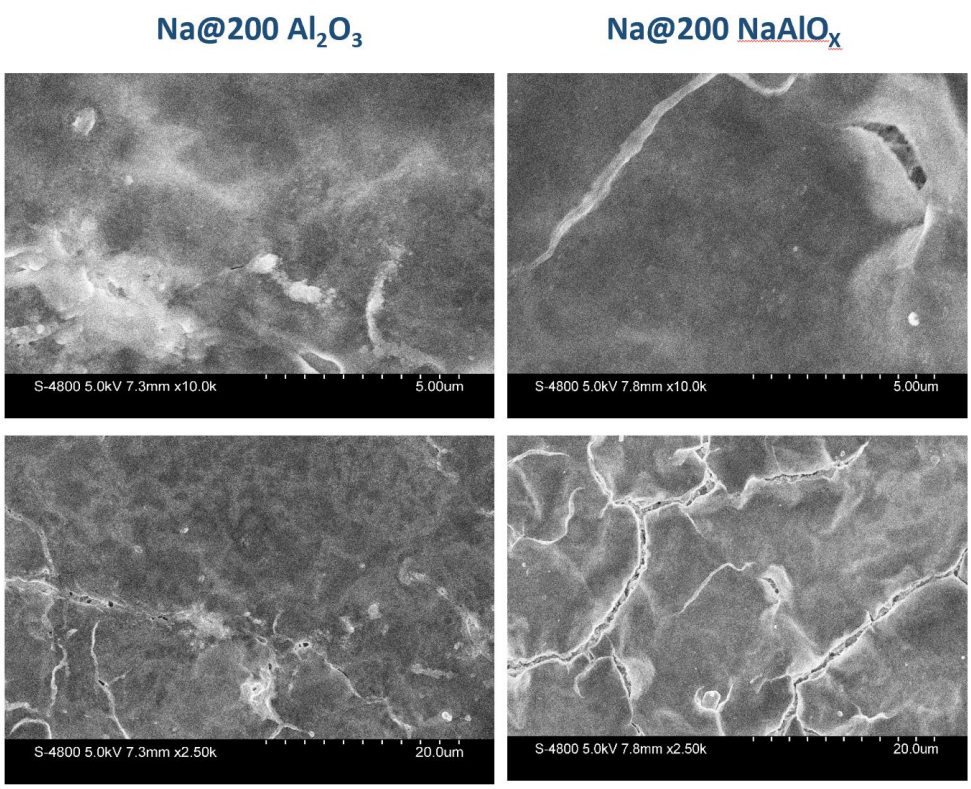


**Fig. S14** Top-view SEM images of Na@200$Al_2O_3$ and Na@200$NaAlO_x$

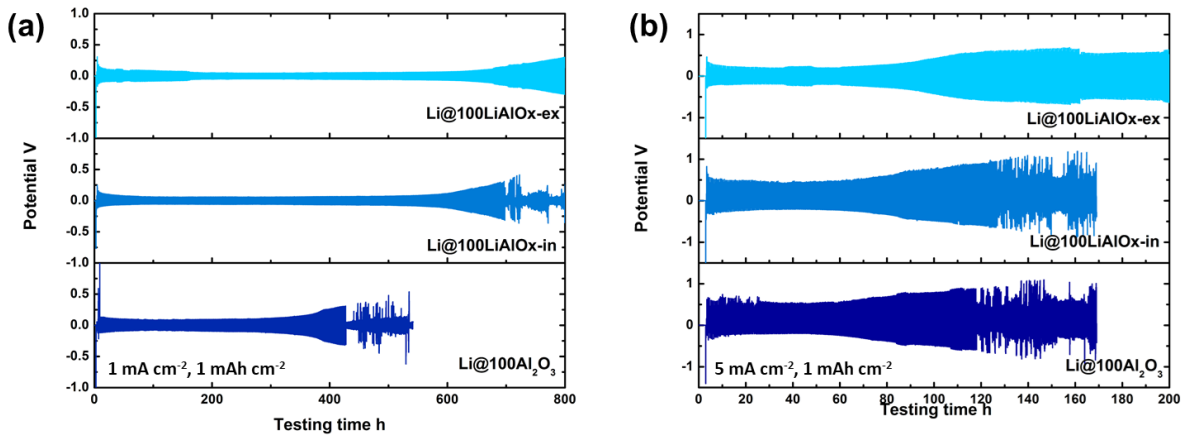


**Fig. S15** The voltage evolution of Li/Li symmetric cells using Li@200$Al_2O_3$, Li@200$LiAlO_x$-ex, and Li@200$LiAlO_x$-in in carbonate-based electrolyte: (a) current density: 1 mA $cm^{-2}$, capacity: 1 mAh $cm^{-2}$; (b) current density: 5 mA $cm^{-2}$, capacity: 1 mAh $cm^{-2}$.

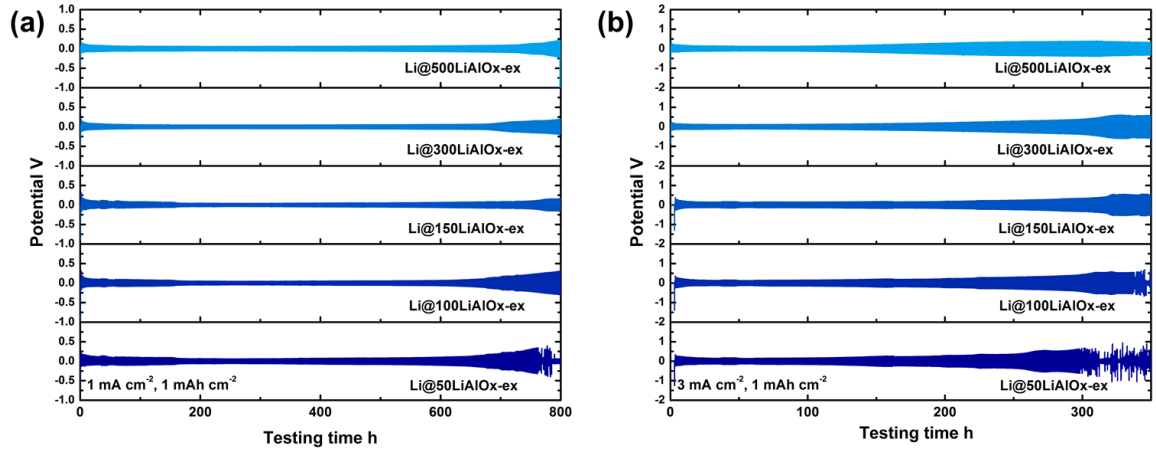


**Fig. S16** The voltage evolution of Li/Li symmetric cells using Li@nLiAlO$_x$-ex (n=50, 100, 150, 300, 500) in carbonate-based electrolyte: (a) current: 1 mA cm$^{-2}$, capacity: 1 mAh cm$^{-2}$; (b) current: 3 mA cm$^{-2}$, capacity: 1 mAh cm$^{-2}$.

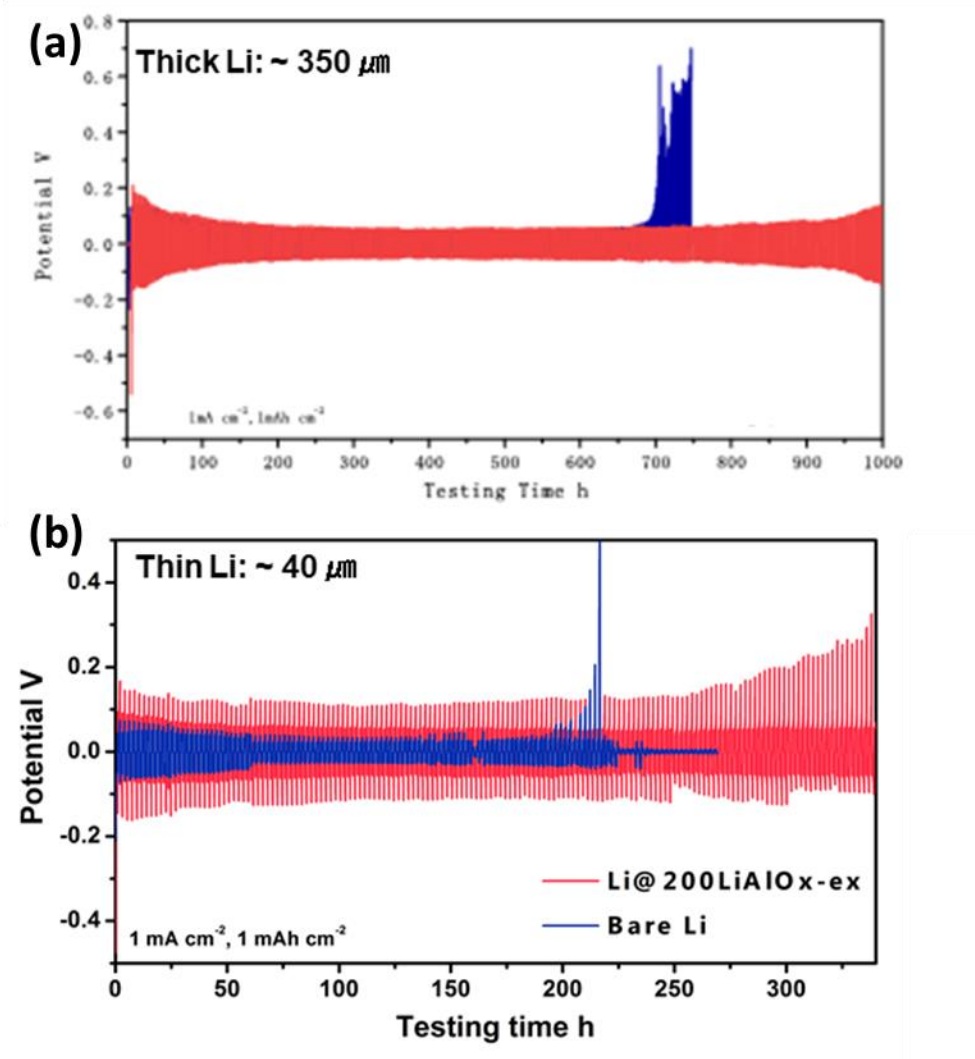


**Fig. S17** The overpotential of Li/Li symmetric cells using bare Li foil and Li@200LiAlOx-ex in carbonate-based electrolyte at the current density of 1 mA $cm^{-2}$ with the capacity of 1 mAh $cm^{-2}$ with (a) thick Li foil (~350 μm) and (b) thin Li foil (~40 μm).

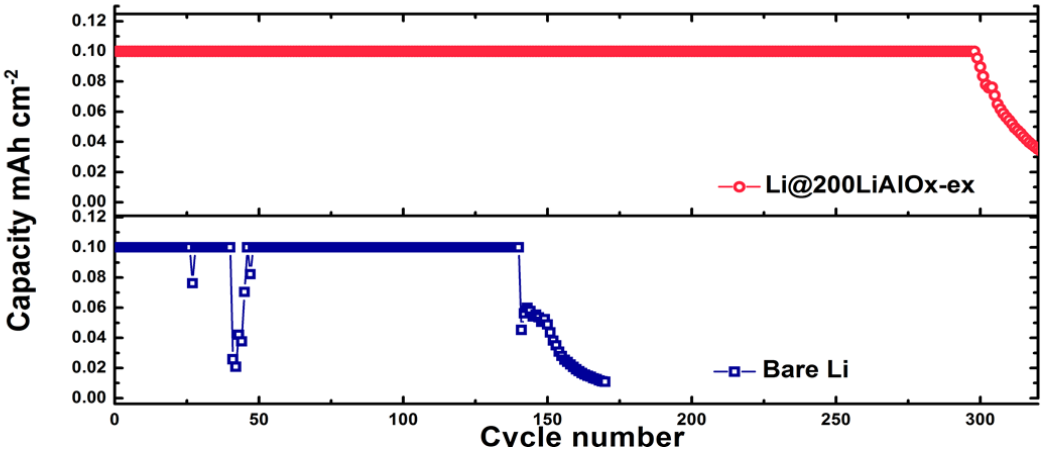


**Fig. S18** Cycling performances of Li-$O_2$ full cells using bare Li foil and Li@200LiAl$O_x$-ex as anode electrode at the current density of 0.1 mA $cm^{-2}$.

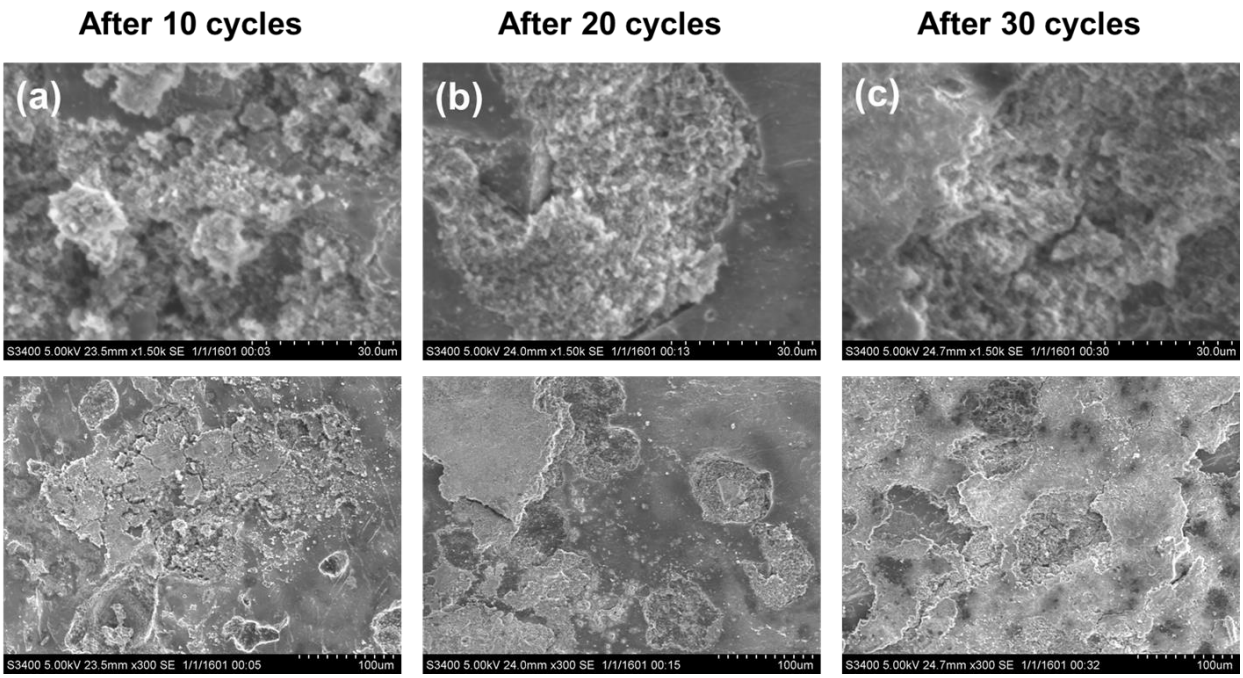


**Fig. S19** Top-view SEM images of bare Li foil after electrochemical plating/striping in carbonate-based electrolyte at the current density of 1 mA $cm^{-2}$ with the capacity limit of 1 mAh $cm^{-2}$, (a) after 10 cycles, (b) after 20 cycles, (c) after 30 cycles.

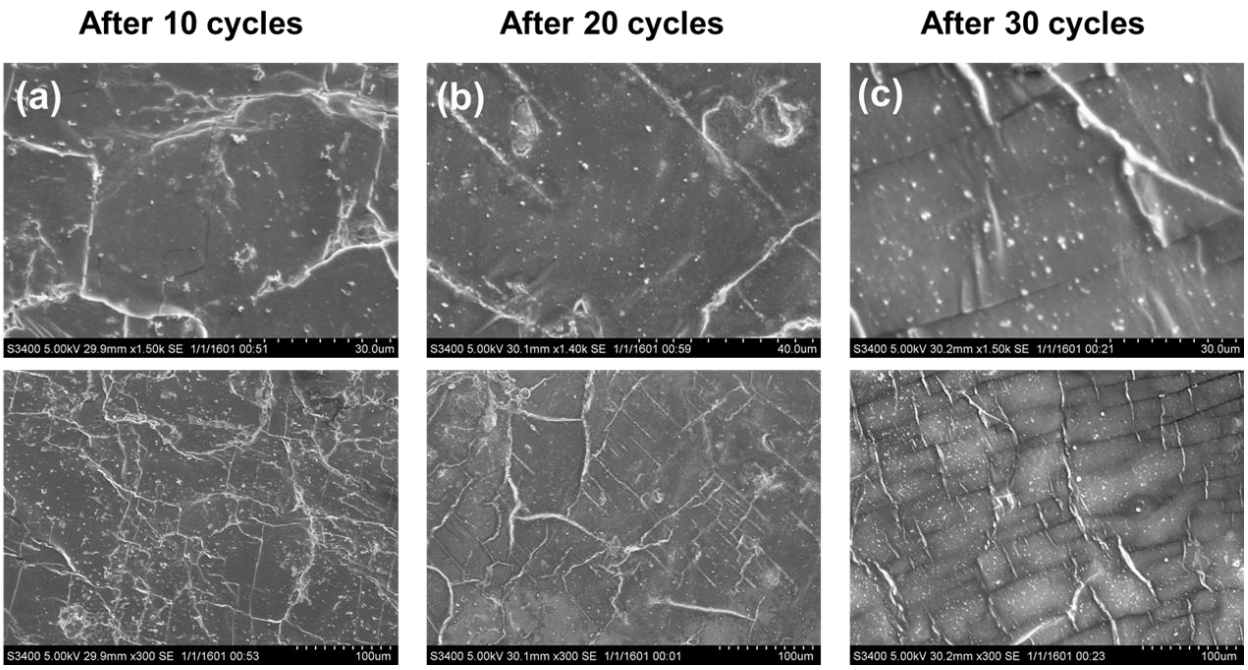


**Fig. S20** Top-view SEM images of Li@200LiAlO$_x$-ex after electrochemical plating/striping in carbonate-based electrolyte at the current density of 1 mA cm$^{-2}$ with the capacity limit of 1 mAh cm$^{-2}$. (a) after 10 cycles, (b) after 20 cycles, (c) after 30 cycles.

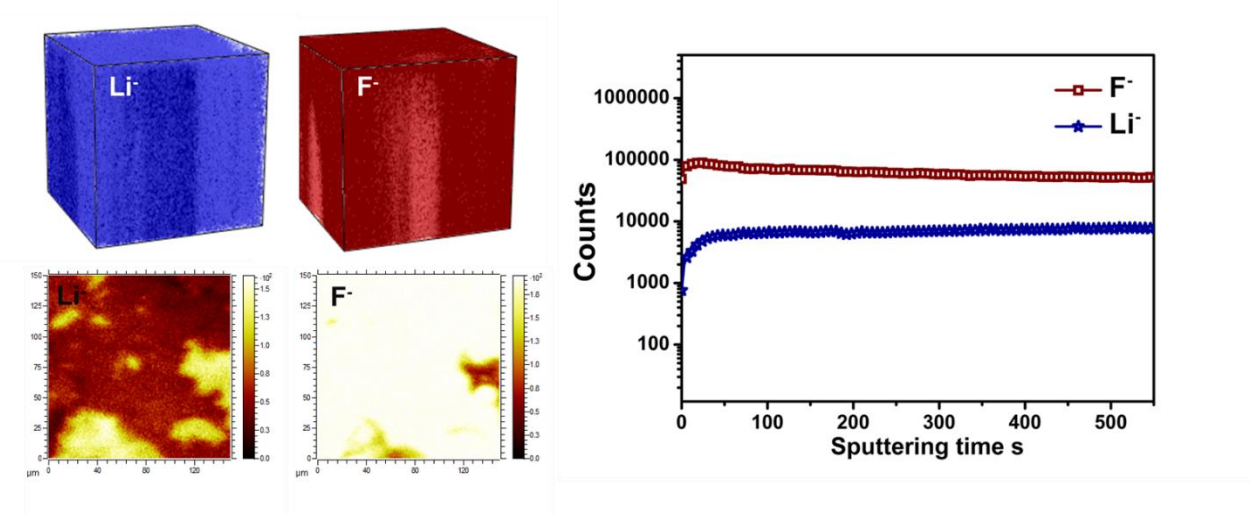


**Fig. S21** The TOF-SIMS 3D reconstructed images, mappings, and depth profiles of bare Li foil after electrochemical cycling (20 cycles) in carbonate-based electrolyte at the current density of 1 mA $cm^{-2}$ with the capacity limit of 1 mAh $cm^{-2}$.

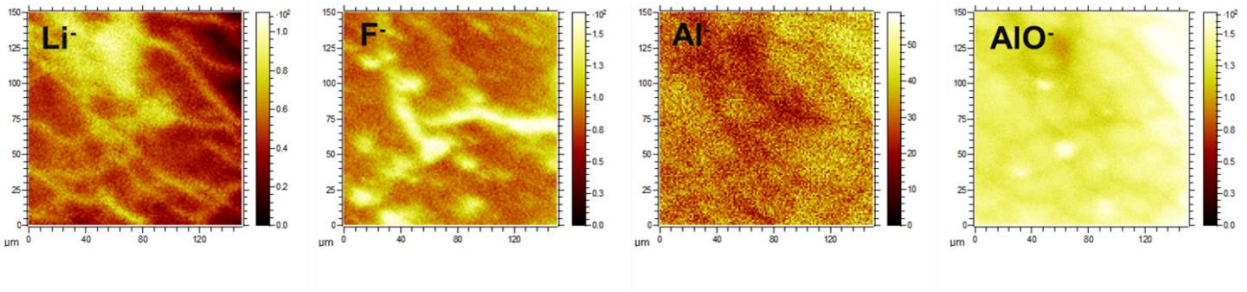


**Fig. S22** The TOF-SIMS secondary ion images of $Li^{-}$, $F^{-}$, $Al^{-}$, and $AlO^{-}$ for Li@200LiAlO$_x$-ex after electrochemical cycling (20 cycles) in carbonate-based electrolyte at the current density of 1 mA cm$^{-2}$ with the capacity limit of 1 mAh cm$^{-2}$.

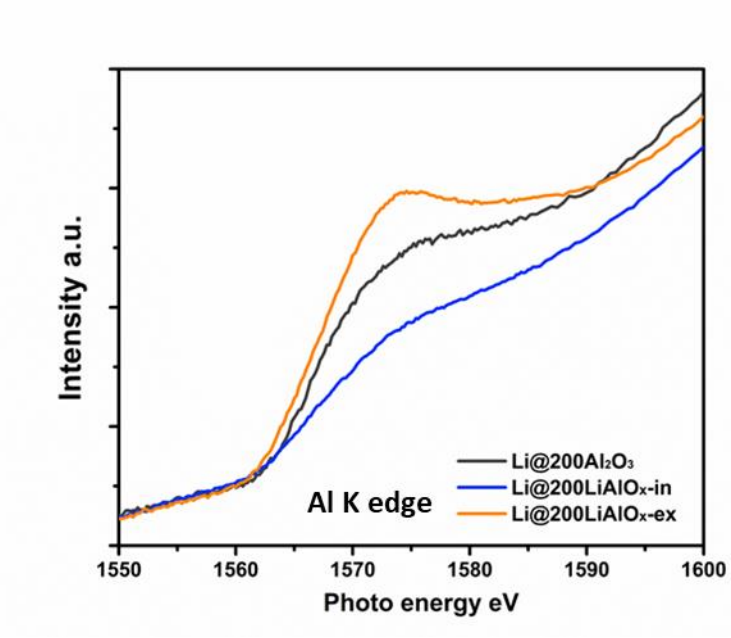


**Fig. S23** The XASENS Al K edge of Li@200$Al_2O_3$, Li@200$LiAlO_x$-ex, and Li@200$LiAlO_x$-in after electrochemical cycling (10 cycles) in carbonate-based electrolyte at the current density of 1 mA $cm^{-2}$ with the capacity limit of 1 mAh $cm^{-2}$.

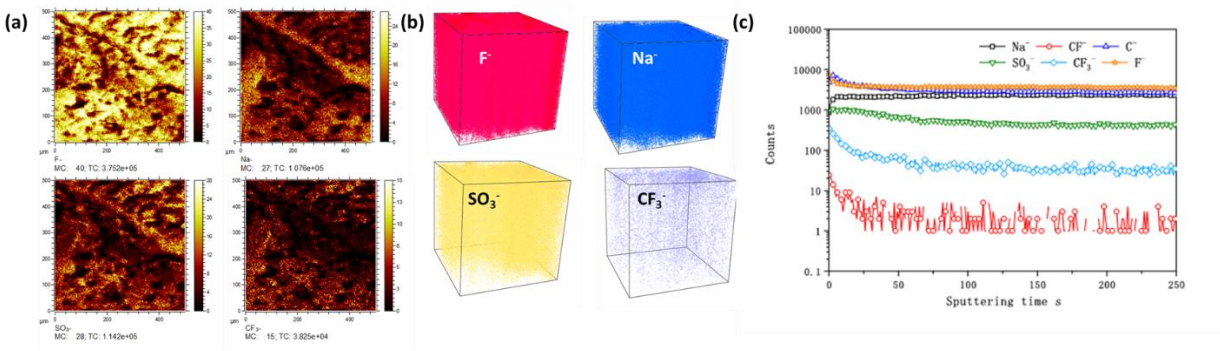


**Fig. S24** The TOF-SIMS surface secondary ion images (a) , depth profile (c) of various secondary ion species and corresponding 3D images (b) of bare Na after cycling.

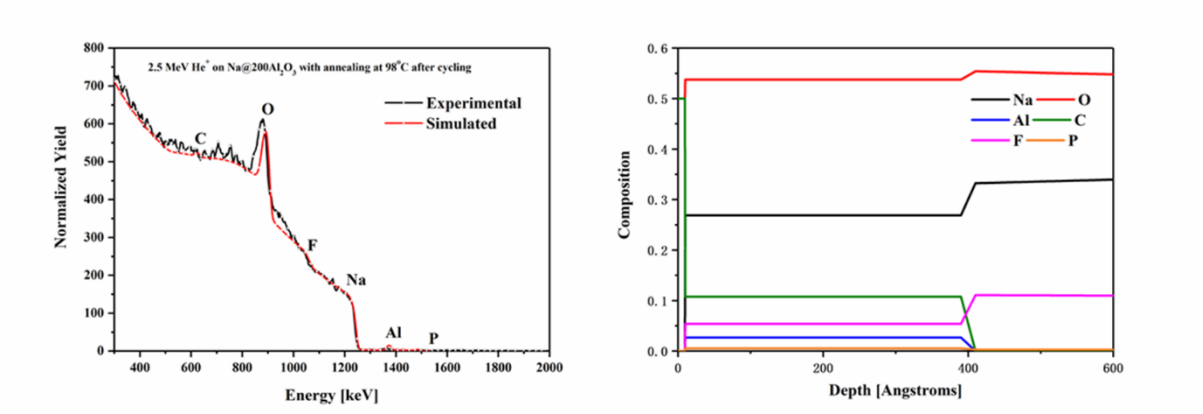


**Fig. S25** The RBS spectra and calculated depth profiles of Na@200NaAlO$_x$ after cycling

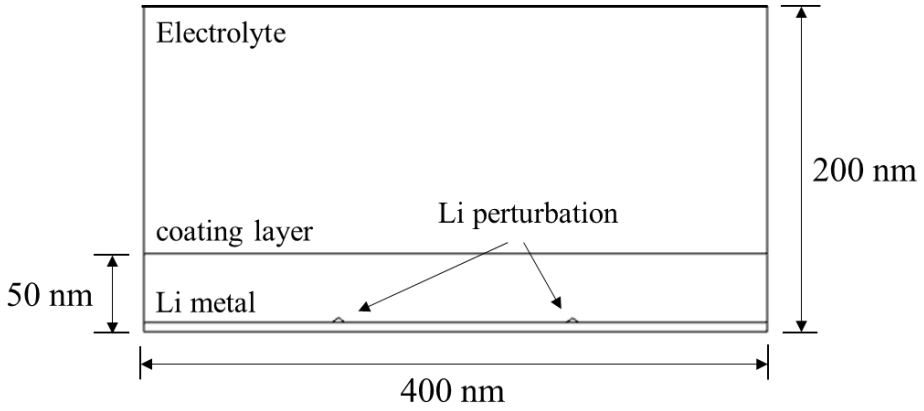


**Fig. S26** The geomtry for phase-field electrodeposition modeling.

References

[1] Yang Zhao,Xiaofei Yang,Liang-Yin Kuo,Payam Kaghazchi,Qian Sun,Jianneng Liang,Biqiong Wang,Andrew Lushington,Ruying Li,Huamin Zhang,Xueliang Sun, High Capacity, Dendrite-Free Growth, and Minimum Volume Change Na Metal Anode, Small, 2018, 14, 1703717

[2] Lei Chen, Hao Wei Zhang, Lin Yun Liang, Zhe Liu, Yue Qi, Peng Lu, James Chen, Long-Qing Chen, Modulation of dendritic patterns during electrodeposition: A nonlinear phase-field model, Journal of Power Sources, 2015, 300, 376-385,